

A Method for Correcting Fourier Transform Spectrometer (FTS) Dynamic Alignment Errors

M.W. Kelly and D.L. Mooney

MIT Lincoln Laboratory
244 Wood St.
Lexington, MA 02420

1. ABSTRACT

The Cross-track Infrared Sounder (CrIS), like most Fourier Transform spectrometers, can be sensitive to mechanical disturbances during the time spectral data is collected. The Michelson interferometer within the spectrometer modulates input radiation at a frequency equal to the product of the wavenumber of the radiation and the constant optical path difference (OPD) velocity associated with the moving mirror. The modulation efficiency depends on the angular alignment of the two wavefronts exiting the spectrometer. Mechanical disturbances can cause errors in the alignment of the wavefronts which manifest as noise in the spectrum. To mitigate these affects CrIS will employ a laser to monitor alignment and dynamically correct the errors. Additionally, a vibration isolation system will damp disturbances imparted to the sensor from the spacecraft. Despite these efforts, residual noise may remain under certain conditions. Through simulation of CrIS data, we demonstrated an algorithmic technique to correct residual dynamic alignment errors. The technique requires only the time-dependent wavefront angle, sampled coincidentally with the interferogram, and the second derivative of the erroneous interferogram as inputs to compute the correction. The technique can function with raw interferograms on board the spacecraft, or with decimated interferograms on the ground. We were able to reduce the dynamic alignment noise by approximately a factor of ten in both cases. Performing the correction on the ground would require an increase in data rate of 1-2% over what is currently planned, in the form of 8-bit digitized angle data.

Key Words: Fourier Transform Spectrometer, Michelson Interferometer, Infrared Sounder

2. BACKGROUND

CrIS will fly as part of the National Polar-orbiting Operational Environmental Satellite System (NPOESS). The first satellite is scheduled for launch around 2010. NPOESS is a tri-agency venture between NOAA, NASA, and DoD, which merges civilian (POES) and defense (DMSP) polar meteorological satellite programs onto a single platform. The NPOESS satellites will eventually replace both two-satellite constellations. The NPOESS constellation will operate in an 833 km, 98.7° inclination, near sun-synchronous orbit. In 1999, ITT Industries in Ft. Wayne, IN was awarded the contract to build CrIS, the atmospheric sounder. The interferometer is being built by ABB Bomem in Quebec City. Meeting demanding noise performance requirements mandates careful sensor design to achieve a detection-limited system.^{1,2} One potential concern with the CrIS is residual noise due to mechanical disturbances imparted to the Michelson interferometer from within the sensor and spacecraft to which it is affixed.

Mechanical disturbances cause dynamic errors in the velocity and alignment of the moving mirror within the interferometer. Dynamic velocity fluctuations cause the signal frequency to jitter slightly during the time an interferogram is collected. A small error in the interferogram is produced due to small changes in the frequency response of electrical components in the signal chain. This error is mitigated by isolating the sensor from mechanical disturbances and by proper electrical design. Dynamic alignment (DA) fluctuations cause the modulation efficiency to jitter during the time an interferogram is collected. A small error in the interferogram is produced due to these gain fluctuations. This error is mitigated by isolating the sensor from mechanical disturbances and by implementing a control system to maintain alignment. The current study focuses on DA errors, and potential algorithmic correction techniques.

This work was sponsored by the Department of the Air Force under Air Force Contract No. F19628-00-C-0002.

Opinions, interpretations, conclusions and recommendations are those of the author and are not necessarily endorsed by the United States Government.

2.1 The Modulation Interferogram

The modulated interferogram, $I(z)$, produced at the output of the CrIS sensor can be written:

$$I(z) = c \int_0^{\infty} S(u, z) \cos(2\pi u + \phi) du \quad (2.1)$$

$$c = \frac{1}{2} A \Omega \tau \rho G_A \quad \text{and} \quad S(u, z) = B(u) F(u) H(u, V(z)) M(u, \beta(z)).$$

$S(u, z)$ is the product of the incident radiance (scene plus background), $B(u)$, times the instrument response function, $F(u)$, the magnitude of the band pass frequency response, $H(u, V(z))$, and the modulation efficiency, $M(u, \beta(z))$. $I(z)$ is integrated over all input optical frequencies, u and given as a function of the moving mirror position, z . The mirror position is tracked using a visible or near-infrared laser reference system. The output of the narrow frequency laser radiation through the interferometer is a sinusoidal function of z . The interferogram is sampled at constant position intervals, i.e., at the zero-crossings of the laser sinusoid. The constant, c , in equation (2.1) includes the aperture area (A), field of view (Ω), peak transmittance (τ), detector responsivity (ρ), and electronics gain (G_A) of the instrument. The instrument response function, $F(u)$, is the total spectral response of the instrument due to optics, filters, and the detector. The electrical frequency out of the detector, f , given wavenumber, u , is the product of the wavenumber times the optical-path-difference (OPD) velocity, V , $f = uV$. The phase, ϕ , is relative to the laser reference signal and contains all shifts due to electronics and any error in the estimated zero path distance reference, ZPD, i.e., the $z = 0$ point. The modulation efficiency is a gain term derived from angular alignment of the wavefronts, $\beta(z)$, combined at the output of the interferometer.

2.2 Dynamic Alignment Errors

The modulation efficiency is a function of both wavenumber and mirror position when mechanical disturbances are uncontrolled within the interferometer. The jitter term is derived by calculating the dip in the mean intensity over a circular exit aperture due to an angle between the two interfering wavefronts:

$$M(u, \beta(z)) = \frac{2J_1(2\pi u \beta(z))}{2\pi u \beta(z)}. \quad (2.2)$$

The argument of the Bessel function, J_1 , contains the wavefront tilt $\beta(z)$, the stop radius, a , and the wavenumber. On CrIS, $\beta(z)$ is expected to be less than 10 microradians, the stop radius is 4 cm, and the maximum wavenumber is 2500 cm^{-1} . The maximum argument of the Bessel function using these values is approximately 0.0628. The Bessel function can then be expanded using a power series to:

$$2 \frac{J_1(\Psi)}{\Psi} = \sum_{k=0}^{\infty} \frac{(-\Psi^2/4)^k}{k!(k+1)!} \approx 1 - \frac{\Psi^2}{8} + \frac{\Psi^4}{192} \dots \quad (2.3)$$

We drop the third and higher terms which do not contribute much to the summation. Neglecting dynamic velocity errors, the expanded expression for the modulated interferogram becomes:

$$I(z) \approx c \int_0^{\infty} B(u) F(u) H(u) \left[\cos(2\pi u) \left(1 - \frac{(\pi a)^2 \beta(z)^2 u^2}{2} \right) \right] du. \quad (2.4)$$

The tilt angle, β , is the root sum of the x-tilt, β_x , and y-tilt, β_y , components:

$$\beta^2(z) = \beta_x^2(z) + \beta_y^2(z). \quad (2.5)$$

Each component is assumed to be a normally distributed random function. The last term in equation (2.4) is a non-linear error caused by a time dependent alignment disturbance. The error is proportional to the square of the

wavenumber and the square of the wavefront tilt angle. The modulated interferogram can be written in terms of the error free interferogram, $I_o(z)$, plus an error term $\delta I(z)$.

$$I(z) = I_o(z) + \delta I(z), \quad (2.6)$$

$$\delta I(z) \approx -c \frac{[\pi a \beta(z)]^2}{2} \int_0^\infty B(u) F(u) H(u) u^2 \cos(2\pi z u) du \quad (2.7)$$

The objective of this work is to recover $I_o(z)$ given $I(z)$ and $\beta(z)$, i.e, determine $\delta I(z)$ and add it to $I_o(z)$.

3. SIMULATION OF RAW AND DECIMATED CRIS INTERFEROGRAMS

In the absence of the appropriate CrIS data for development of DA jitter correction techniques[‡], we used an existing interferogram simulator. It is a computer simulation written in MATLAB, and closely emulates data collected from engineering units. Additionally, some phenomena not expected to manifest in the sensor, but potentially problematic for correction techniques were included to test the robustness of the correction. The simulation included the effects of photon shot noise, electronics noise, 1/f noise, response non-linearity, optical dispersion, background flux, self-apodization due to the use of an extended (on-axis) detector, ghosting, and quantization. Sampling errors due to dynamic velocity fluctuations were not included in this stage of development. Interferograms were constructed directly in the time domain and dimensioned as the true operational CrIS interferograms.

CrIS can collect a raw interferogram from each detector in three spectral bands every 200 milliseconds. There are nine detectors per spectral band. The bands cover between 650 – 2552 cm^{-1} , and are classified as long-wave (LW), mid-wave (MW), and short-wave (SW) infrared bands. Raw interferograms are detected with HgCdTe detectors, amplified, filtered, and digitized. The raw interferograms are intentionally highly over-sampled to minimize quantization noise and high frequency noise aliasing. The over-sampled interferograms are decimated (digitally filtered with a complex FIR digital filter, and then down-sampled) for communication to the ground. Table 3.1 gives the raw sampling and decimation parameters for each band.

Table 3.1 CrIS Raw Interferogram Sampling and Decimation Parameters

	BAND		
	LW	MW	SW
Band (cm^{-1})	650-1095	1210-1750	2155-2550
Maximum OPD (cm)	± 0.8035	± 0.4092	± 0.2015
Sampling Interval (nm)	775	775	775
Raw Samples (N)	20736	10560	5200
Digitization (bits)	14	12	12
Decimation Factor (K)	24	20	26
Decimated Samples (L)	864	528	200

In this work, we simulated LW band interferograms, several mechanical disturbance scenarios, and correction performance for three possible implementations. Figure 3.1 shows the simulated raw and decimated interferograms and the associated spectra. The scene radiance used to generate the interferograms was simulated from mid-latitude TIGR data. The spectra are calculated directly by Fast Fourier Transforms (FFTs) of the simulated interferograms. In each case the appropriate shift was applied to the spectra for presentation.

[‡] Earlier feasibility work demonstrated key concepts using SW data collected at Telops Inc.

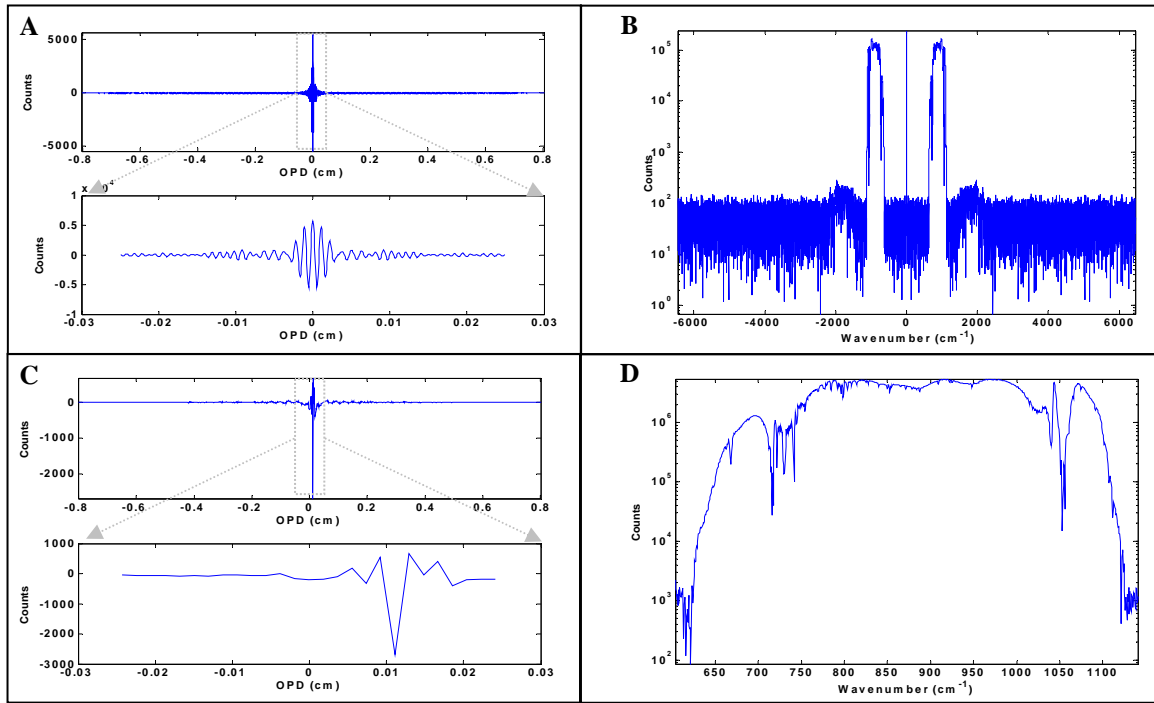


Figure 3.1 Simulated A. raw interferogram, B. raw spectrum C. decimated interferogram, and D. decimated spectrum. Interferograms are shown over the full OPD range and expanded around the peak.

The complex FIR filter used in the simulation was similar to the filter that will be used operationally, but perhaps lower performing. Figure 3.2 shows the magnitude response of the filter plotted vs. wavenumber, along with the real and imaginary coefficients, b , plotted vs. index number, n . The CrIS LW band is indicated with lines between 650 and 1095 cm^{-1} . The filter provides approximately 62 dB suppression of out-of-band noise prior to the down-sampling operation. After filtering the interferogram is down-sampled by 24 to produce an 864 element, complex interferogram.

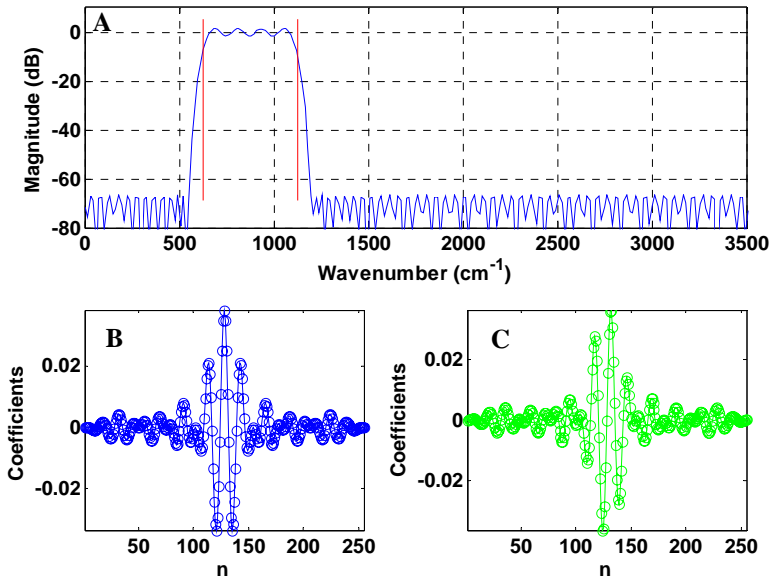


Figure 3.2 A. Magnitude of the complex FIR Filter applied to the interferogram prior to down-sampling. B. Real and C. Imaginary coefficients.

Six mechanical disturbance cases were considered in this work. The DA wavefront power spectra for each scenario are shown in Figure 3.3. Power spectra centered at baseband were derived by low-pass filtering a random error with a 4-pole Butterworth filter. The -3 dB cutoff was set to 15 Hz, 150 Hz, and 250 Hz. The band-limited spectra were then modulated at 450 Hz to simulate a tone. The RMS error for each case was approximately $5\text{--}10 \times 10^{-6}$ radians. In addition to the dynamic error, an 8×10^{-6} radian static error was simulated. Simulated angle data were noise-free and quantized between 6- and 12-bits to model down-linked data. All computations were 64-bit floating point operations.

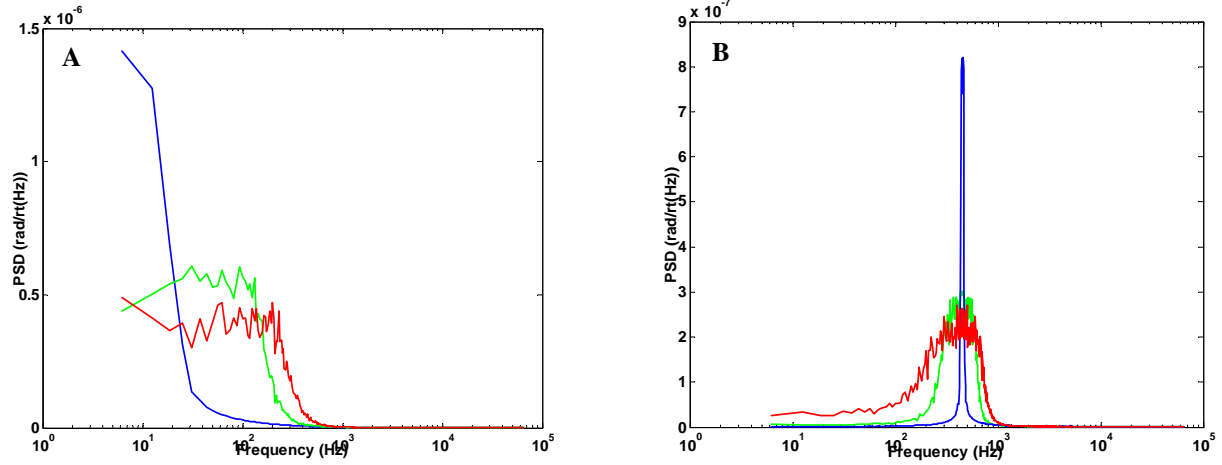


Figure 3.3. DA error jitter spectra for six case studies considered in this work: 15, 150, and 250 Hz centered at baseband (A) and at 450 Hz (B). The RMS error for each case was between 5 and 10 microradians.

The effectiveness of the correction can be determined by comparing the spectral noise for uncorrected and corrected interferograms to the jitter-free case. In each case, the simulation followed the CrIS two-point complex calibration procedure described in [3]. The reference blackbody radiances used for calibration were 0°C and 37°C. The noise equivalent delta radiance, NEdN, was calculated as the standard deviation of the calibrated spectra in each spectral bin. Figure 3.4 shows the calculated NEdN for DA jitter case, and the case with no jitter. Detector noise dominates the NEdN when DA jitter is not present. Twenty interferograms were considered in each case. Additionally, the noise correlation matrix was calculated to determine the mechanism of the dominant noise source in each spectral bin. Unlike

detector or electronics noise, which in general are uncorrelated, dynamic alignment jitter noise is highly correlated from channel to channel. Figure 3.5 shows a graphical image representation of the noise correlation matrix for three case studies: No DA jitter, 150 Hz Baseband jitter, and 150 Hz jitter modulated at 450 Hz. In each case, the matrix diagonal is identically one (deep red). Random noise is completely uncorrelated between channels and, if dominant, the matrix value is zero (deep blue). DA jitter noise is highly correlated and, if dominant, the matrix value is one (deep red). Dynamic alignment errors are dominant throughout most of the spectrum when not corrected.

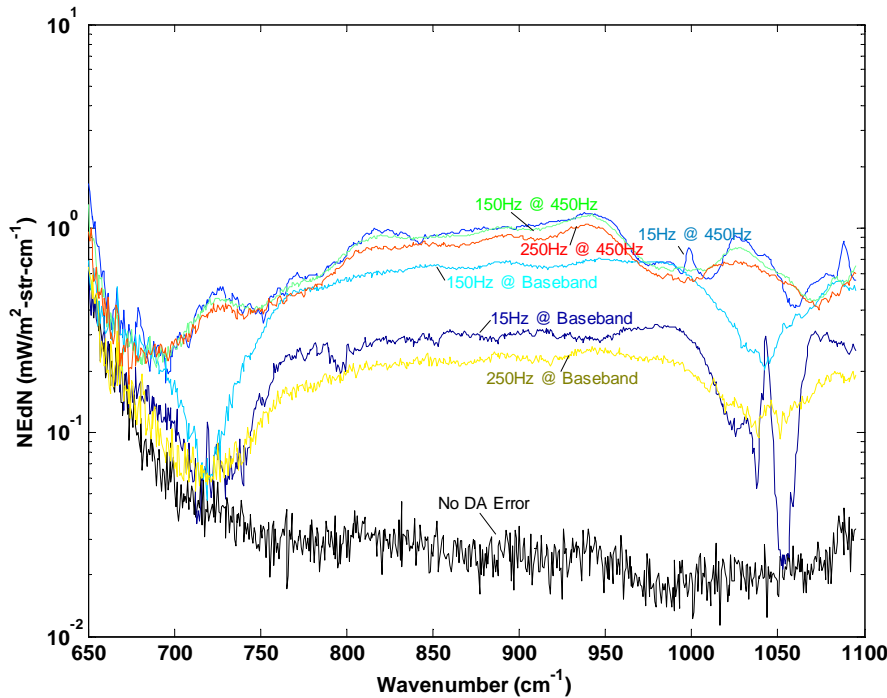


Figure 3.4 NEdN of interferograms corrupted with dynamic wavefront alignment jitter. The NEdN is plotted for the case when no error is present (black) and each of the jitter power spectra described in section 3.

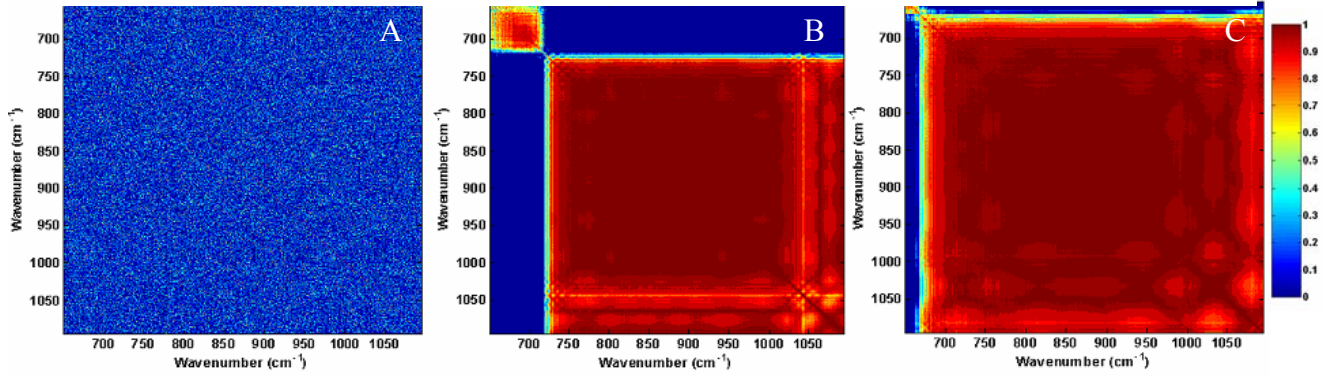


Figure 3.5 Graphical representation of the noise correlation matrix for 3 representative DA jitter cases: A. no jitter, B. 150 Hz baseband jitter, and C. 150 Hz jitter modulated at 450 Hz.

4. CORRECTION ALGORITHM

There are three opportunities for implementation of a correction algorithm in the data processing sequence:

1. On-board before decimation.
2. On-board after decimation.
3. On the ground after decimation.

On-board the spacecraft, prior to decimation, one has access to the raw interferogram and angles to make a correction. After decimation, two options exist: up-sample and recover the original measured interferogram as closely as possible, or operate directly on the decimated interferogram.

4.1 Approximation of the DA Error on Raw Interferograms

From equation (2.7), the DA error at each point in the spectrum is proportional to the angle $\beta(z)$ multiplied by the second derivative of the discrete, error free interferogram, $I_o''(z)$. The measured, discrete interferogram can be formally written in terms of the second derivative of I_o :

$$I(n) = I_o(n) + I_o'' \frac{a^2 \beta(n)^2}{8}, \quad I_o'' = \frac{\partial^2 I_o}{\partial^2 z}(n) \quad (4.1)$$

For small errors, the measured interferogram can be used in place of the error free interferogram to approximate the second derivative, forming the basis of the correction technique. A numerical technique was used to compute the second derivative, and the error free interferogram can be approximately recovered from:

$$I_o(n) \approx I(n) + \zeta(n), \quad \zeta(n) = -\frac{a^2 \beta(n)^2}{8} \frac{[I(n-1) + I(n+1) - 2I(n)]}{\Delta z^2}, \quad (4.2)$$

where $\zeta(n)$ is the correction term ($\zeta(n) \approx \delta I(n)$). The advantage of this approach is that it is well defined and simple. It can be performed on-board, in real time with only a one-sample delay. The disadvantage is that it must operate on the high rate data. The approach requires a good estimate of the derivative, which is achievable with over-sampled interferograms. Figure 4.1 shows the correction for the case of 250 Hz band-limited jitter centered at baseband. The “measured” error (black line) is determined by differencing the corrupted interferogram with a jitter-free interferogram. The correction (red points), calculated using equation (4.2), is also plotted, showing a good match. The plot is shown around the interferogram peak, where the error is the greatest. The correction far away from the peak, and where the wavefront alignment is good, is small compared with the noise.

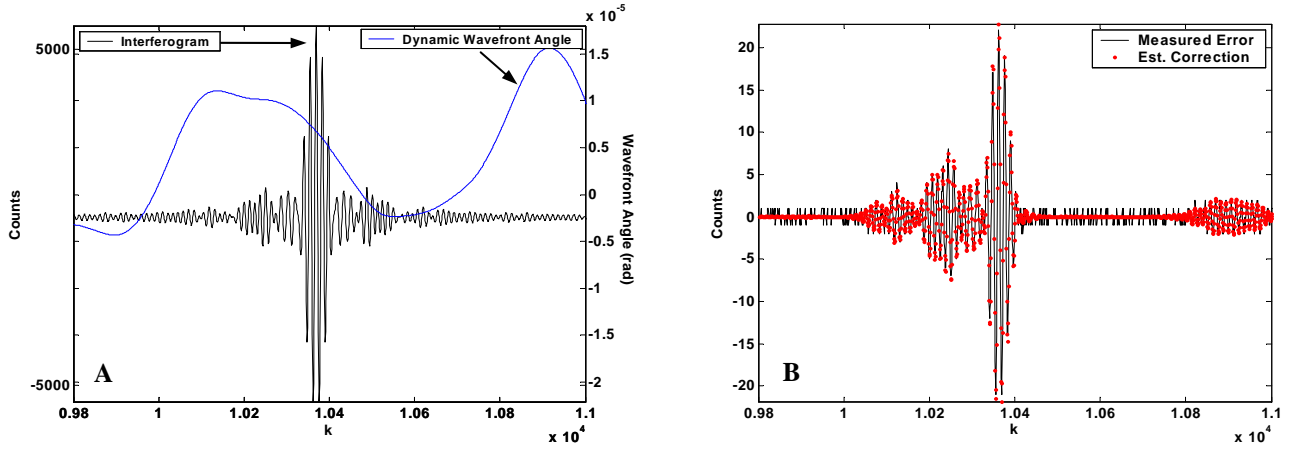


Figure 4.1 A. An interferogram (black) plotted with the 250 Hz wavefront angle (blue), around the ZPD peak. B. The measured error (black line) compared with the calculated correction (red points).

4.2 Approximation of the DA Error on Decimated Interferograms

The decimation process is designed to deliberately alias the spectral content of the interferogram to a narrower range in a way that allows unambiguous reconstruction of the spectrum. The band-limited discrete-time interferogram $I_b(n)$, is a convolution of the measured interferogram and the filter coefficients:

$$I_b(n) = \sum_{m=0}^{N_F} b(m)I(n-m) , \quad (4.3)$$

where N_F is the filter length. By substituting equation (4.1) into the above equation, we can estimate $I_b(n)$ from:

$$I_b(n) \approx \sum_{m=0}^{N_F} b(m)I_o(n-m) + \sum_{m=0}^{N_F} b(m) \frac{(\pi a)^2 \beta(n-m)^2}{8} \frac{\partial^2 I_o}{\partial^2 z}(n-m) \quad (4.4)$$

The decimation process is completed by down-sampling $I_b(n)$ by the decimation factor, K . If the extent of the filtered signal spectra is less than the sampling frequency of the re-sampled sequence, the entire spectrum is shifted to the new baseband. The down-sampled and filtered interferogram, $I_d(n)$, is given by:

$$I_d(n) = I_b(nK) \quad (4.5)$$

$$\approx \sum_{m=0}^{N_F} b(m)I_o(nK-m) + \frac{(\pi a)^2}{8} \sum_{m=0}^{N_F} b(m)\beta(nK-m)^2 \frac{\partial^2 I_o}{\partial^2 z}(nK-m)$$

After decimation, implementing the correction technique becomes more complex. The technique described in section 4.1 does not work directly with decimated interferograms. The simple, numerical second derivative calculation fails when using under-sampled data. We tested two options to mitigate this problem:

1. Recover the original, undecimated interferogram as closely as possible and proceed as described in section 4.1.
2. Use an analytical method for calculating the second derivative directly from the decimated interferogram.

4.2.1 Up-Sampling to Recover an Estimate of the Undecimated Interferogram

We recovered an estimate of the undecimated spectrum by up-sampling the decimated interferogram (with zeros) by the decimation factor K , and scaling by K :

$$I_{us}(nK) = KI_d(n), \quad L-1 < n < 0 \quad (4.6)$$

$$I_{us}(n) = 0, \quad \text{otherwise}$$

where L is the length of the decimated interferogram sequence and $I_{us}(n)$ is the up-sampled interferogram sequence of length $N=KL$. The original, undecimated spectrum was then estimated by windowing the associated spectrum:

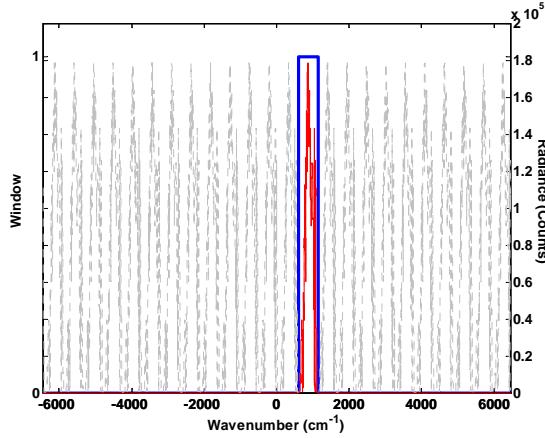


Figure 4.2 Spectrum of the up-sampled decimated interferogram (grey) and the portion remaining after filtering (red) with a simple window (blue).

$$\hat{S}(k) = W(k) \frac{1}{N} \sum_{n=0}^{N-1} I_{us}(n) e^{-i2\pi \frac{nk}{N}}, \quad (4.7)$$

where $W(k)$ is a window defined as:

$$W(k) = \begin{cases} 1, & k_{low} < k < k_{high} \\ 0, & otherwise \end{cases} \quad (4.8)$$

The low and high indices defining the window, k_{low} and k_{high} , were derived from the width of the decimated spectrum:

$$k_{low} = \frac{u_{low}}{du} + \frac{N}{2}, \quad k_{high} = \frac{u_{high}}{du} + \frac{N}{2}, \quad (4.9)$$

where $u_{low} = 602 \text{ cm}^{-1}$ is the minimum wavenumber in the decimated spectrum, $u_{high} = 1142 \text{ cm}^{-1}$ is the maximum, and $du = 0.6223 \text{ cm}^{-1}$ is the spectral bin size of the undecimated spectrum. Figure 4.2 shows the operation graphically. The resulting estimate is an over-sampled spectrum nearly identical

to the original (less the out of band noise, etc.). An estimate of the original, undecimated interferogram was then recovered by deconvolving the digital filter coefficients, b :

$$I(n) \approx \hat{I}(n) = \frac{2}{N} \cdot \text{real} \left[\sum_{k=0}^{N-1} \hat{S}(k) \sum_{j=0}^{N-1} b^{-1}(j) e^{i2\pi \frac{(n-j)k}{N}} \right]. \quad (4.10)$$

The estimate was phase shifted by the length of the filter, N_f , which must be accounted for prior to jitter correction, but otherwise a good estimate of $I(n)$. The correction was calculated from $\hat{I}(n)$ as described in section 4.1.

4.2.2 Computing the Correction Directly on the Decimated Interferogram and Angles

As previously stated, if the extent of the filtered signal spectra is less than the sampling frequency of the re-sampled sequence, the entire spectrum is shifted to the new baseband. Furthermore, if the maximum frequency of the tilt errors is small compared to the width of the filter window, it can be treated as a constant in the convolution, and the filtered interferogram can be written:

$$I_b(n) \approx \sum_{m=0}^{N_f} b(m) I_o(n-m) + \frac{(\pi a)^2 \beta(n - N_f/2)^2}{8} \sum_{m=0}^{N_f} b(m) \frac{\partial^2 I_o}{\partial^2 z}(n-m). \quad (4.11)$$

The angle is delayed by $N_f/2$ to account for a phase in the filtered spectrum. This technique should be effective for low frequency disturbances, less than half the sampling rate divide by the filter length, $F_s/(2 N_f) \approx 250 \text{ Hz}$. The decimated interferogram can then be written:

$$\begin{aligned} I_d(n) &\approx \sum_{m=0}^{N_f} b(m) I_o(nK - m) + \frac{(\pi a)^2 \beta(nK - N_f/2)^2}{8} \sum_{m=0}^{N_f} b(m) \frac{\partial^2 I_o}{\partial^2 z}(nK - m) \\ &\approx I_{o,d}(n) + \frac{(\pi a)^2 \beta(n - N_f/2)^2}{8} \frac{\partial^2 I_{o,d}(n)}{\partial^2 z}. \end{aligned} \quad (4.12)$$

Like the previous case (correction of full-length interferograms), the errors are small, so we estimate the noise free decimated interferogram $I_{o,d}(n)$ with the measured, decimated interferogram, $I_d(n)$.

$$I_{o,d}(n) \approx I_d(n) + \zeta_d(n), \quad \zeta_d(n) = -\frac{(\pi a)^2 \beta(nK - N_f/2)^2}{8} \frac{\partial^2 I_d(n)}{\partial^2 z}. \quad (4.13)$$

Calculating the correction, $\zeta_d(n)$, requires an estimate of the down-sampled derivatives of the continuous interferogram from the discrete form. The p^{th} derivative of the continuous interferogram from the undecimated discrete version is given by

$$\frac{d^p I}{dx^p}(n) = \sum_{m=0}^{N-1} \left(i2\pi \frac{k}{N} \right)^p S(k) e^{i2\pi \frac{nk}{N}}. \quad (4.14)$$

The spectrum of the p^{th} derivative, $S^{(p)}(k)$, is derived from the discrete version of the continuous spectrum, $S(k)$, from:

$$S^{(p)}(k) = \sum_{n=0}^{N-1} \frac{d^p I}{dx^p}(n) e^{i2\pi \frac{nk}{N}} = \left(i2\pi \frac{k}{N} \right)^p S(k). \quad (4.15)$$

In general, the utility of this approach depends on the noise in the continuous signal and the quantization accuracy. For the interferogram correction discussed here, the noise levels are low enough for the first and second derivatives to be accurately computed. When the interferogram has been down-sampled, an estimate of the derivatives proceeds the same way, but the location of a spectral components must be identified in the *original spectrum* and multiplied by a powers $i2\pi(k-1)/N$ in the *original spectrum*. Suppose $N=KL$ is the size of the original interferogram. The decimated spectrum, $S_d(k)$, is directly transformed from the decimated interferogram by:

$$S_d(k) = \frac{1}{L} \sum_{n=0}^{L-1} I_d(n) e^{-i2\pi \frac{nk}{L}} = \frac{1}{L} \sum_{n=0}^{L-1} I_b(nK) e^{-i2\pi \frac{nk}{L}}. \quad (4.16)$$

$I_b(k)$ was substituted from equation (4.5). The original, filtered spectrum, $S_b(k)$, is obtained from the filtered interferogram by:

$$I_b(n) = \sum_{k=0}^{N-1} S_b(k) e^{i2\pi \frac{nk}{N}}. \quad (4.17)$$

Substituting, we get the down sampled spectrum in term of the original spectrum

$$\begin{aligned} S_d(k) &= \frac{1}{L} \sum_{j=0}^{N-1} S_b(j) \sum_{n=0}^{L-1} e^{i2\pi \frac{n(j-k)}{L}} = \sum_{j=0}^{N-1} S_b(j) \delta(j-k)_{Mod L} \\ &= \sum_{q=0}^{K-1} S_b(k + q \cdot L) \end{aligned} \quad (4.18)$$

The estimate of the down-sampled spectrum of the p^{th} derivative of the original continuous interferogram is therefore:

$$S_d^{(p)}(k) = \sum_{j=0}^{K-1} \left(i2\pi \frac{k + j \cdot L}{N} \right)^p S_b(k + j \cdot L), \quad (4.19)$$

and the estimated p^{th} order decimated derivative of the original continuous interferogram is

$$\frac{d^p I_d}{dx^p}(n) = \sum_{k=0}^{M-1} S_d^{(p)}(k) e^{i2\pi \frac{nk}{M}}. \quad (4.20)$$

It is essential to note that we are estimating the down-sampled derivative not the derivative of the down-sampled interferogram. Figure 4.3 shows an example of the real and imaginary decimated corrections for the case of 250 Hz band-limited jitter centered at baseband, compared to the “measured” error (black line) for both correction methods discussed above. The “measured” error was computed by differencing the corrupted, decimated interferogram with a jitter-free, decimated interferogram in the simulation. The correction calculated by up-sampling the corrupted interferogram and angles, and then decimating the results is plotted in red (points). The correction calculated directly on the decimated interferogram and angles is plotted in green (circles). Both compare favorably to the measured error with a small difference at the peak.

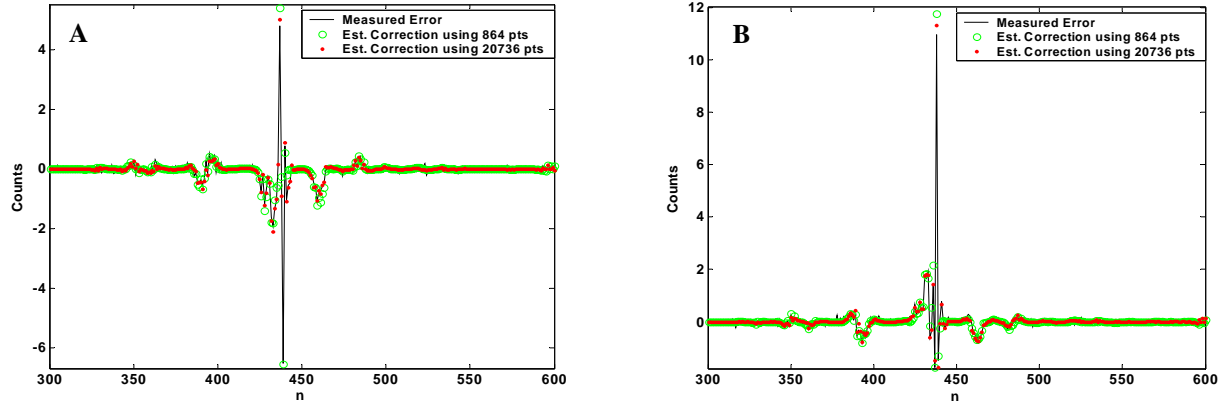


Figure 4.3 Real (A) and imaginary (B) errors, 1. measured (black line), 2. calculated by up-sampling the corrupted interferogram and angles, then decimated (red points), and 3. calculated directly on the decimated interferogram and angles (green circles)

5. RESULTS

We performed 72 case studies, examining six jitter power spectra (described in section 3), three correction methods (described in section 4), and four angle digitization scenarios (6-, 8-, 10-, and 12-bit resolution). To simplify the evaluation, the results were classified using two simple figures of merit: 1. the *mean* noise ratio of the case at hand to the jitter-free case, and 2. the *mean* of the correlation matrix (including the diagonal). These figures of merit do not necessarily determine the usefulness of an approach, but provide a method for evaluating results quickly and easily. Before an approach is implemented on CrIS, a more detailed analysis should be performed. The results for all case studies are tabulated and compared to uncorrected and jitter-free interferograms in Table 5.1.

Table 5.1 Mean NEdN ratio and mean correlation for all jitter correction case studies, a case with no jitter present, and a case when no correction was applied to the corrupted interferogram. Highlighted cases are plotted below.

Mean NEdN Ratio							Mean Correlation						
Jitter PSD	15Hz @ 0Hz	15Hz @ 450Hz	150Hz @ 0Hz	150Hz @ 450Hz	250Hz @ 0Hz	250Hz @ 450Hz	15Hz @ 0Hz	15Hz @ 450Hz	150Hz @ 0Hz	150Hz @ 450Hz	250Hz @ 0Hz	250Hz @ 450Hz	
No Jitter	1.00	1.00	1.00	1.00	1.00	1.00	0.00	0.00	0.00	0.00	0.00	0.00	
No Correction	8.20	26.88	17.78	26.11	6.59	23.84	0.48	0.83	0.48	0.85	0.51	0.86	
6 bit Angle Digitization	Method 1	1.50	3.19	1.97	3.51	1.23	3.53	0.33	0.61	0.44	0.64	0.10	0.70
	Method 2	1.51	3.14	1.99	3.46	1.23	3.49	0.33	0.61	0.44	0.65	0.10	0.70
	Method 3	1.56	6.94	2.21	6.73	1.79	6.31	0.31	0.19	0.43	0.17	0.12	0.20
8 bit Angle Digitization	Method 1	1.10	2.82	1.49	2.86	1.13	2.85	0.07	0.56	0.32	0.52	0.03	0.54
	Method 2	1.11	2.78	1.51	2.81	1.14	2.81	0.07	0.56	0.32	0.53	0.03	0.54
	Method 3	1.10	6.87	1.69	6.64	1.66	6.27	0.04	0.14	0.21	0.14	0.02	0.12
10 bit Angle Digitization	Method 1	1.11	2.74	1.42	2.74	1.17	2.73	0.08	0.53	0.30	0.49	0.07	0.50
	Method 2	1.12	2.69	1.44	2.69	1.17	2.70	0.08	0.54	0.30	0.49	0.07	0.50
	Method 3	1.11	6.85	1.63	6.64	1.69	6.28	0.07	0.13	0.15	0.13	0.04	0.12
12 bit Angle Digitization	Method 1	1.13	2.72	1.41	2.71	1.18	2.71	0.09	0.53	0.29	0.48	0.08	0.50
	Method 2	1.14	2.67	1.43	2.66	1.18	2.67	0.09	0.53	0.29	0.48	0.08	0.50
	Method 3	1.12	6.86	1.63	6.64	1.70	6.28	0.09	0.13	0.15	0.13	0.05	0.11

Correction Method 1 refers to the correction discussed in section 4.1, before decimation. Correction Method 2 refers to the technique discussed in section 4.2.1, after decimation and up-sampling the spectrum to use a numerical second derivative.

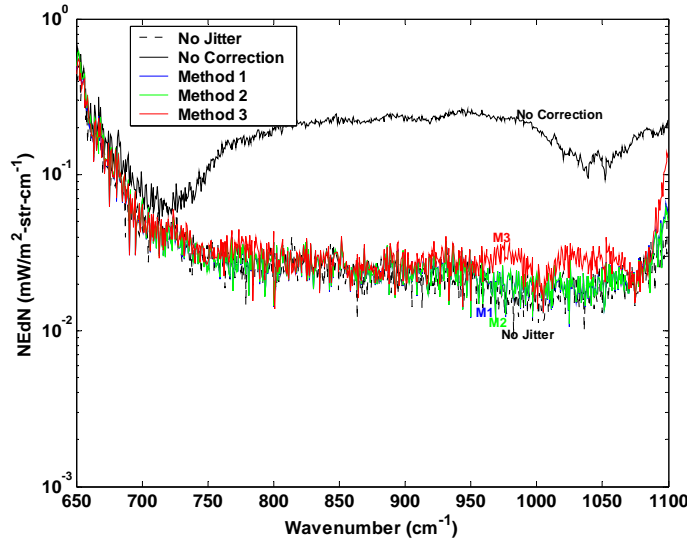


Figure 5.1 NEDN of interferograms corrupted with 250 Hz band-limited at baseband jitter before correction (black solid) after correction Method 1 (blue), after correction Method 2 (green), and after correction Method 3 (red). Also plotted is the NEDN of jitter-free interfereferograms (black dotted).

digitized with 8-bit resolution. Figure 5.1 shows the NEDN of interferograms corrupted with 250 Hz band-limited jitter at baseband before correction (black solid) after correction Method 1 (blue), after correction Method 2 (green), and after correction Method 3 (red). Also plotted is the NEDN of jitter-free interferograms (black dotted). The corrections all reduce the noise down to the jitter-free case. There is a small increase in noise around 950 – 1050 cm^{-1} when Method 3 was used. Figure 5.2 shows a graphical representation of the noise correlation matrix for each correction method. Some areas of strong noise correlation exist between 950 and 1100 cm^{-1} when Method 3 is used to correct jitter errors. All other regions for all three methods are uncorrelated, indicating the correction reduced the errors below the detector/electronics (white) noise floor.

Correction Method 3 refers to the technique discussed in section 4.2.2, after decimation and calculating the second derivative analytically on the down-sampled interferogram. The results indicate very good correction results in all cases, between 4- and 12- times noise reduction. When the noise was confined to baseband the corrections were able to get within a factor of two of the jitter-free noise when angles were digitized with 8- or more bits. There was a slight fall-off when 6-bit resolution was used. When a tone was simulated, the correction still reduced the noise by about a factor of ten, but only achieved the noise floor to within a factor of approximately three. Again, digitizing with more than 6-bits produced slightly better results. As expected, Method 3 had more difficulty with the higher frequency jitter cases.

The NEDN after correction is plotted for one jitter case, highlighted in Table 5.1, along with the uncorrected and jitter-free NEDN cases. The noise correlation matrix is also shown graphically. Each correction used angles

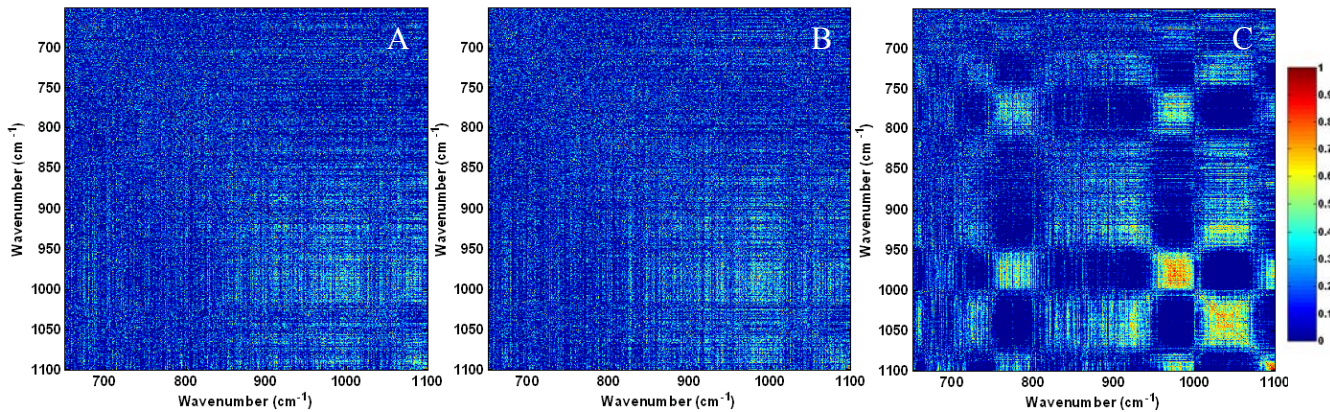


Figure 5.2 Graphical representation of the noise correlation matrix after correcting 250Hz band-limited jitter at baseband using: correction Method 1 (A), Method 2 (B) and Method 3 (C).

6. SUMMARY

Mechanical disturbances imparted to the Michelson interferometer within the CrIS sensor can cause errors in the alignment of the interfering wavefronts. These dynamic alignment fluctuations cause the modulation efficiency to jitter during the time an interferogram is collected, and manifest as noise in the measured spectrum. The disturbances may originate from within the sensor or from other mechanisms on the spacecraft to which it is affixed. To mitigate these affects CrIS will employ a laser to monitor and dynamically correct low frequency errors. A vibration isolation system will damp higher frequency disturbances imparted to the sensor from the spacecraft. Despite these efforts residual noise may remain under certain conditions and so a method for correcting DA noise is desirable.

This work demonstrates an algorithmic technique to correct DA errors. The technique requires only the time-dependent wavefront angle, sampled coincidentally with the interferogram, and the second derivative of the erroneous interferogram as inputs to compute the correction. The technique can function with raw interferograms on board the spacecraft, or with decimated interferograms on the ground. Two methods for calculating the correction on decimated interferograms were explored, recovering an estimate of the raw interferogram to compute the numerical second derivative, and computing it analytically directly on the under-sampled data. The analytical technique is much less computationally intense, but only functions well with low-frequency jitter, less than about 250 Hz. We tested all three methods using simulated CrIS data. We evaluated the noise statistics of the calibrated spectra, the standard deviation in each spectral bin and noise correlation matrix, to determine the effectiveness of each approach. All three techniques were able to reduce the dynamic alignment jitter noise by approximately a factor of ten when the noise was band-limited to less than 250 Hz. When the noise was modulated with a 450 Hz tone, computing a correction directly on the decimated interferogram did not work as well, as expected, but still reduced the noise by a factor of about four.

The correction could be implemented either on-board the spacecraft or before calibration algorithms are applied to the data during ground processing. There are drawbacks and benefits to each approach. A system level trade study considering, the correction algorithm performance, the required amount of data communicated to the ground, and the computing power required on-board should determine the eventual implementation strategy. On-board the spacecraft, prior to decimation, there is access to the raw (20736 LW points) interferogram and angles to make a correction. Both correction methods after decimation (864 LW points) require an FFT calculation, and practically would only be implemented on the ground. Ground processing may require a small amount of additional data communicated to the ground in the form of digitized DA angles. The exact amount of data required depends on the frequency and resolution of the digitized data.

The current simulation was performed with DA angles digitized to 6-, 8-, 10-, and 12-bits. There was approximately a 25% improvement in the performance of the correction between 6- and 8-bits digitization, and no improvement thereafter. The simulation provided the exact coincident angle at every point in the raw interferogram, and decimated angles when correcting decimated interferograms. Both interferograms and angles were decimated by the same factor in this study, 24. Using this benchmark, and considering CrIS collects 34 interferograms every 8 seconds, it is possible to make the correction on the ground with an increase of about 29 kbps. This represents less than 2% increase in the total data rate (1.5 Mbps). Although not demonstrated here, it may be possible to further reduce the data rate (by a factor of 2 or more) by down-sampling the angle data to the Nyquist rate prior to down-link.

7. ACKNOWLEDGEMENTS

This work was sponsored by the Department of the Air Force under Air Force Contract No. F19628-00-C-0002.

8. REFERENCES

1. K. Schwantes, D.Cohen, P. Mantica, R. Glumb, *SPIE Proceedings*, p. 456-463, Vol. 4486, 2002
2. R. J. Glumb, D.C. Jordan, P. Mantica, *SPIE Proceedings*, p. 411-424, Vol. 4486, 2002
3. Revercomb, H. E., H. Buijs, H. B. Howell, D. D. LaPorte, W. L. Smith, and L. A. Sromovsky. *Applied Optics*, Vol. 27, pp. 3210-3218, 1988.